DOI: 10.1002/anie.201105283

Nanocapsules

Highly Active Nanoreactors: Nanomaterial Encapsulation Based on Confined Catalysis**

Marcos Sanlés-Sobrido, Moisés Pérez-Lorenzo, Benito Rodríguez-González, Verónica Salgueiriño, and Miguel A. Correa-Duarte**

Considerable efforts have been devoted to the fabrication of nanomaterials with well-defined morphologies for specific applications. This is the case of nanocapsules that simultaneously provide the advantages of hollow and porous systems. They can consequently be used as storage spaces or reaction chambers while supplying the necessary paths for the design of controlled uptake/release systems.[1–3] Particular interest in the performance of chemical reactions in these confined environments has led to catalyst-containing hollow nanocapsules, so that a diffusional product/substrate exchange between the inner cavity and the bulk solution takes place in an efficient way. Clearly, the nature of the interface, as well as the inner and outer surface properties of these nanoreactors, appear to be critical factors to modulate the catalytic activity of the whole system.

Synthetic strategies for nanocapsules include self-assembly and subsequent cross-linking of pre-formed nanosized objects,[4] or direct reactive routes such as interfacial polymerization with reagents dissolved in different liquid phases.[5] This latter approach requires soluble precursors in both the dispersed and the continuous solvent phase. Thus, they can react at the interface and yield the desired shell but this condition also constrains the possible precursors to employ. Additionally, because capsules should be permeable to numerous reagents, their applications as nanoreactors will depend on the controllable uniform porosity at the molecular scale, a feature that in fact would enable the fabrication of size-selective microreactors.[6] To fulfill this requirement we have chosen silicon oxide (SiO_2).[7] Indeed, depending on the method exploited for its precipitation, networks of uniform but different pores of molecular dimensions can be provided.[8,9]

The main driving force prompting the exploration of nanocapsule systems is based on their large and uniform porosity, underlying their remarkable potential in such diverse areas as biomedicine,[10–12] gas storage,[13] catalysis,[14–16] or adsorptive separation.[17,18] Their successful application depends on the availability of the synthetic methods to prepare defect-free capsules so that permeation does not occur as a result of uncontrolled porosity through gaps or cracks, but solely through the existing channels.

The nanocapsule activity and the properties of their permeable membrane have been widely reported, but few reports exist regarding a catalyst located in the nanocavity.[19–24] In fact, examples of catalyst-containing nanoreactors are scarce and no close attention has been paid to the degradation of the catalyst activity during their encapsulation. Thus, more effort should be made in this direction.

Given the special relevance of every of the different features underlined, we have developed nanoreactors endowed with high catalytic activity. These systems are based on the previous encapsulation of singular dendritic Pt nanoparticles (Pt_d NPs) located in the hollow empty space enclosed by porous silica nanocapsules. It is worthy to point out that this synthetic approach helps to preserve the catalytic activity of the catalyst, even after their encapsulation. Thus, the single-crystal Pt_d NPs will catalyze specific reactions to take place inside the silica porous shell. As it is the shell that allows the product/substrate exchange between the inner cavity and the bulk solution, the reaction becomes confined and controlled inside the nanoreactors. To verify this potential and the efficacy as a nanoreactor, an electron-transfer process was chosen as a test reaction. Additionally, the system was successfully brought into play for the production of Ni/NiO nanostructures with different magnetic behavior, in view of the controlled reactions carried out in the inner cavity. This finding opens the door to an engineered capsules fabrication to modulate the inclusion and possible isolation of different inorganic materials.

The hollow capsules were fabricated by means of an initial polymer functionalization in a similar way to that described in the literature.[25,26] It commonly comprises the coating of the surface template particles (polystyrene (PS) in our case) with charged polyelectrolytes. The stepwise adsorption of these polyelectrolytes reverses the charge on the surface template and aids the deposition of subsequent layers of a wide range of charged components.[20,27–29] Negatively charged Pt_d NPs were therefore driven onto the modified and now positively charged PS template surface (see Experimental Section) to

[*] M. Sanlés-Sobrido, Dr. M. Pérez-Lorenzo, Dr. B. Rodríguez-González, Prof. M. A. Correa-Duarte
Departamento de Química Física—Unidad Asociada CSIC
Universidade de Vigo, 36310 Vigo (Spain)
E-mail: macorrea@uvigo.es
Dr. V. Salgueiriño
Departamento de Física Aplicada
Universidade de Vigo, 36310 Vigo (Spain)
E-mail: vsalgue@uvigo.es

[**] M.P.-L. and V.S. acknowledge the Isidro Parga Pondal and Ramón y Cajal fellowships (Xunta de Galicia and Ministerio de Ciencia e Innovación, Spain). This work has been supported under projects MAT2008-06126 (Ministerio de Ciencia e Innovación), INCITE08PXIB209007PR, INCITE09209101PR, 10PXIB312260PR, 2008/077 and 2010/78 (Xunta de Galicia, Spain) and METACHEM (grant no. CP-FP 228762-2 from the EU).

Supporting information for this article is available on the WWW under http://dx.doi.org/10.1002/anie.201105283.

form PS/Pt_d composites. Subsequently, a controlled silicon oxide precipitation was forced to take place on the surface of the PS/Pt_d composites, permitting the formation of a hybrid and inorganic shell surrounding the initial cores. Finally, the PS core was removed promoting the hollow capsule formation (Figure 1 and Experimental Section). This last step is also crucial for the availability of the Pt_d NPs as catalysts in reactions confined in this evolved empty space, rendering the nanocapsules effective nanoreactors (Pt_d/SiO_2).

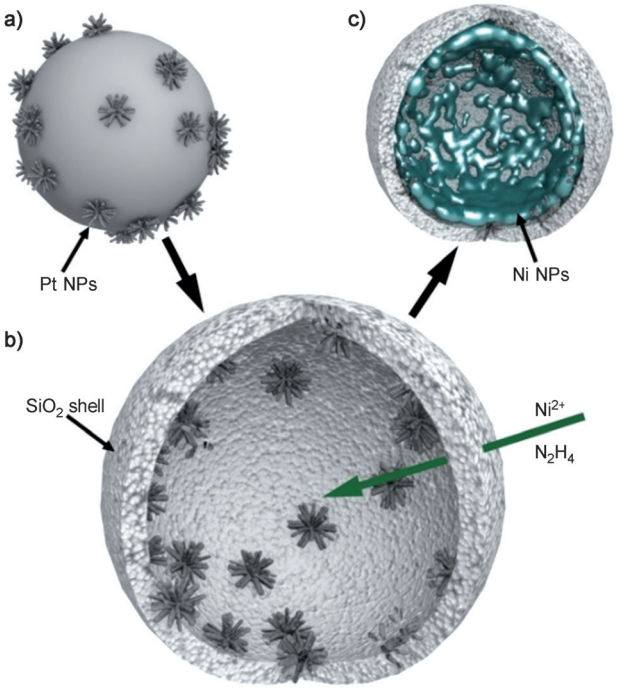

Figure 1. Synthesis of Ni/NiO magnetic nanostructures by controlled reactions carried out in the inner cavity of the previously formed nanoreactor. a) Hybrid particles composed of dendritic Pt NPs deposited onto polystyrene (PS) colloidal templates; b) hollow capsules obtained after the silica coating and polymer dissolution processes; c) formation of magnetic Ni nanomaterial confined inside the silica hollow capsule by reduction of the Ni^{2+} ions using hydrazine and catalyzed with the dendritic Pt NPs.

Figure 2 shows the two-step strategy exploited for the capsule fabrication. Figure 2a includes a TEM image and a model (inset top right) of the Pt_d-coated PS templates. Figure 2b,c,d display images of the obtained hollowed-out Pt-containing nanostructures and a representative model (inset on the top-right of Figure 2b). A higher magnification image (Figure 2d) clearly shows the Pt_d nanoparticles observed through the much lower contrast of the silica shell. These Pt_d nanoparticles, as already reported, are single crystals (Supporting Information, Figure S1).[30] The silicon oxide precipitated uniformly over the entire surface of the Pt_d-coated PS templates and no presence of defects or cracks is observed, even after the PS core dissolution. This consistent and homogeneous silica shell, as a membrane for the nanocapsules, therefore ensures the exchange of reactants and products to take place solely through the pores that make up its chemical disposition.

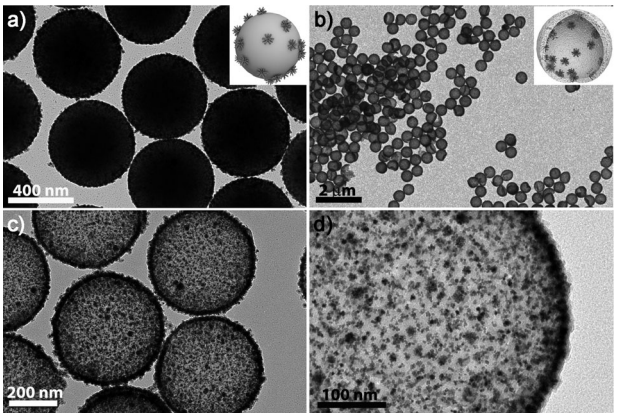

Figure 2. TEM images of a) Pt_d NPs deposited onto PS spheres and b) the hollow capsules obtained after silica coating of hybrid PS/Pt_d particles followed by the etching of the PS core.

Platinum-based nanomaterials are among the most widely used in catalysis. Their activity and selectivity are strongly dependent on composition, size, and shape, and consequently much effort has been devoted in the search for new and more efficient Pt structures.[31–33] Accordingly, redox probe tests with a ferro/ferricyanide system in aqueous solution were conducted in the presence of the hollow (Pt_d/SiO_2) and non-hollow-core (PS/Pt_d) composites reported herein to assess their catalytic activity (see experimental details in the Supporting Information). These reactions were run by first mixing the Pt-based catalysts and sodium borohydride. In the case of hollow capsules, BH_4^- ions diffuse through the pores of silica reacting with the Pt_d NPs to form metal hydrides on their surface. The ability of metal nanoparticles to act as electron acceptors has been previously reported.[30] Thereafter, hexacyanoferrate (III) was added. This complex also migrates through the silica shell to the negatively charged surface of the Pt_d nanoparticles located on the internal wall of the silica membrane. Then, the reduction of the adsorbed $Fe(CN)_6^{3-}$ to $Fe(CN)_6^{4-}$ takes place. Once the final product is formed, it desorbs and diffuses out of the nanoreactor. In this case, the nanoparticle surface would operate as a source of electrons providing the necessary metal active sites for the reaction to proceed.

By plotting the logarithm of the pseudo first-order rate constant (k_{obs}) versus the inverse temperature ($1/T$), the Arrhenius equation was used to determine the activation energy for the Pt_d-catalyzed electron-transfer reaction. Thus, a value of $12.6 \pm 1.2\ kJ\,mol^{-1}$ was obtained for the redox process in the presence of the PS/Ptd composites, while a value of $12.3 \pm 0.8\ kJ\,mol^{-1}$ was achieved for the reaction catalyzed by Ptd/SiO_2 capsules. As the activation energy for the noncatalyzed reaction is $30\ kJ\,mol^{-1}$,[34] the results obtained (Supporting Information, Figure S2) indicate a remarkable catalytic activity of these hybrid nanocomposites.

Accordingly, the catalytic efficiency of the proposed systems was seen when using similar nanostructures but employing 2–3 nm spherical Pt nanoparticles (Pt_s) instead of dendritic ones (for synthetic details, see the Supporting Information). The widely reported and broadly studied Pt_s nanoparticles, synthesized by reduction with $NaBH_4$ and

stabilized through sodium citrate adsorption, can be considered as the model or reference system. PS particles were consequently coated with Pt_s, and their catalytic activity was estimated using the reduction of ferricyanide with sodium borohydride. The energy barrier for this reaction is rather high (30 kJ mol^{-1}) if uncatalyzed,[34] but the presence of PS/Pt(s) composites lowers this value to 17.1 ± 1.1 kJ mol^{-1}. Nevertheless, it must be pointed out that the activation energy reported in the presence of the PS/Pt_d composites (12.6 ± 1.2 kJ mol^{-1}) is significantly lower than that obtained through the widely used 2–3 nm spherical Pt morphology. This tendency is in good agreement with that reported in the literature.[30,33,35]

The high catalytic efficiency found for both systems can be attributed to the presence of Pt_d NPs on the nanocomposites. The defects and under coordinated Pt atoms, commonly found in dendrite-like structures, are considered to be the real active sites in electron-transfer reactions.[35] It must be also noted that the activation energy for the Pt_d/SiO_2 capsules is indistinguishable from that obtained for the PS/Pt_d composites and consistent with the values reported in the literature for dendritic Pt NPs.[30] Accordingly, it can be assumed that the treatment to produce capsules through SiO_2 coating and PS core dissolution has no repercussion on the Pt_d NP morphology and therefore does not affect their catalytic efficiency.

These highly active nanoreactors therefore favor the confined fabrication of nanostructures of very different materials. Hydrazine can reduce nickel ions in the presence of Pt nanoparticles located on the surface of carbon nanotubes[36] or polymer beads.[37] Therefore, we may assume that the Pt_d NPs located in the cavities of the capsule can exert the same degree of catalytic activity giving rise to metallic nickel nanoparticles inside the reactor. Indeed, the porous nature of the silica shell that allows the reactants to reach the nanocavity also permits the Pt-catalyzed reduction to take place in a confined manner.

Figure 3a shows how the integrity of the nanoreactor remains intact after the formation of metallic Ni in its inner cavity (see also the Supporting Information, Figure S3, S4). A higher-magnification TEM image (Figure 3b) over the edge of the hollow hybrid structure reveals the homogeneity of the silica shell (about 10 nm thick) and the growth of the magnetic material inside the nanoreactor. Additionally, a HRTEM analysis of the nanoreactor (Figure 3c) shows the crystalline nature of the magnetic particles formed. Further evidence of the formation of Ni inside the reactor are provided by the EDS spectra (Figure 3d), which clearly show the presence of Ni. Given that Ni^{2+} reduction takes place on the surface of the Pt_d nanoparticles, a layered morphology is obtained. The formation of this layered but still hollow structure was confirmed by XEDS measurements (Figure 3e), with analogous profiles for SiO_2 (blue), Pt (orange), and Ni (green) that point out this kind of morphology. A selected-area electron-diffraction (SAED) pattern (Supporting Information, Figure S3) confirms the presence of metallic Ni, although it does not discount the presence of small amounts of nickel oxide or hydroxide.

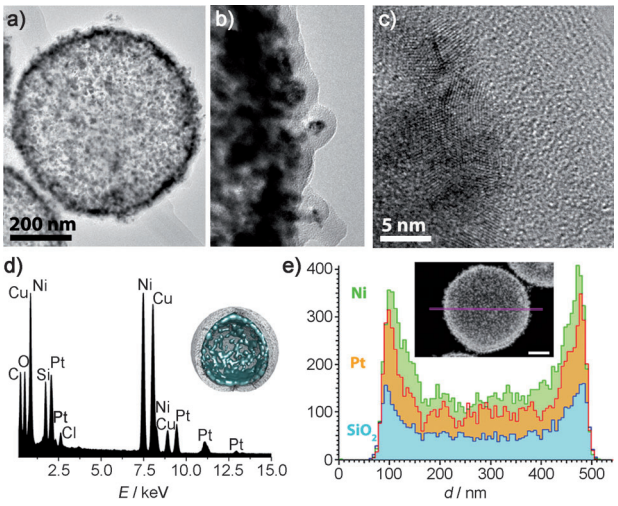

Figure 3. a) TEM image of the Pt_d/SiO_2 nanoreactor after growing nickel inside; b) closer view of the edge of the Pt/SiO_2 membrane; c) HRTEM image of Ni and Pt nanoparticles located in the inner surface; d) EDS spectra; and e) XEDS profiles (determined following the purple line trajectory indicated in the inset TEM image), demonstrating the composition and hollow nature of the capsules. Scale bar in inset: 100 nm.

The amount of nickel reduced inside the capsule can be finely tuned by controlling the Ni^{2+} precursor concentration employed. Thus, capsules with specific amounts of Ni loaded inside were prepared, highlighting their different magnetic behavior. The magnetic nanostructures contained in the hollow capsules were characterized using VSM magnetometry. The magnetic response depends directly on the type of magnetic material formed but also on the size and interactions between the nanostructures attained inside the capsules. The hysteresis loops included in Figure 4a,b ($T = 5$ and 300 K) reflect two main contributions in both samples; one of these is responsible for the large magnetization values owing to ferromagnetic (FM) metallic nickel, which is superimposed on the antiferromagnetic (AFM) linear contribution ($M_a = \chi_a H$, clearly observed at low temperature) responsible for the non-saturation of the magnetization at high field values. This AFM contribution, which is more defined in sample A, corresponds to the nickel oxide and hydroxide magnetic phases identified.

The reason for a higher (or more visible) AFM contribution in sample A can stem from the fact that the magnetic nanoparticles are smaller, which is due to the lower amount of Ni^{2+} precursor employed. Smaller nanoparticles imply an increased surface-to-volume ratio and therefore an increase in the proportion of magnetic material that has become oxidized. This is also reflected in the saturation magnetization (M_0) values at high fields that reach 5 emu g^{-1} for sample A (higher proportion of AFM NiO and/or $Ni(OH_2)$), compared to the 15 emu g^{-1} for sample B (higher proportion of FM Ni). Despite these important values in terms of M_0 for both samples, especially in the case of sample B, they keep the superparamagnetic character regarding the very small almost null coercivity values observed at $T = 300$ K. This nearly superparamagnetic character of the magnetic hybrids under-

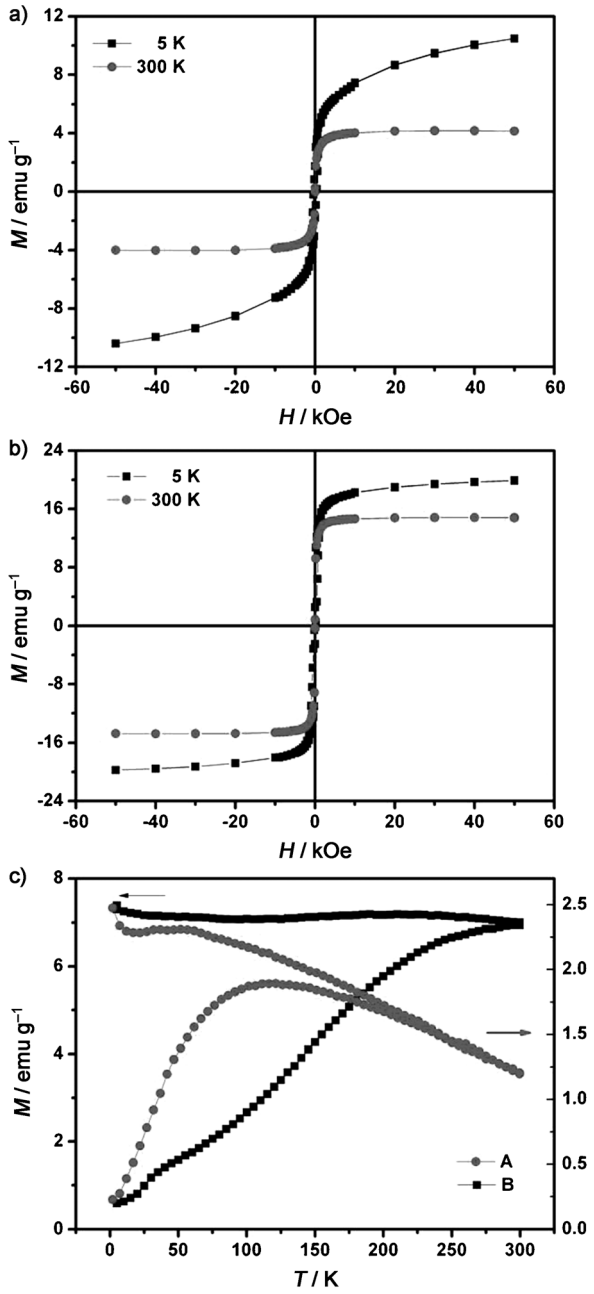

Figure 4. a,b) Field-dependent magnetization curves (at $T = 5$ and 300 K) of sample A (a) and B (b). c) ZFC-FC magnetization curves ($H = 100$ Oe) of A and B.

lines the individuality of the very small nanoparticles formed inside the cavities.

Zero-field-cooled (ZFC) and field-cooled (FC) magnetization curves (Figure 4c) recorded after cooling the samples in zero field and in a small field ($H = 100$ Oe) respectively, from room temperature to 5 K. The ZFC curve corresponding to sample A displays a maximum around 121 K while sample B ZFC curve maximum is located close to but above 300 K. For sample A, both curves coincide at high temperatures and may exhibit a paramagnetic-like decay with increasing temperature, reflecting the superparamagnetic response of the particles within the time window of the measurement technique. With decreasing temperature the curves split; the ZFC reaches the maximum at $T_B = 121$ K, which roughly corresponds to the average blocking temperature of the nanoparticles and decreases thereafter, while the FC curve keeps increasing until it reaches a plateau.

The main reason for a markedly different T_B is usually related to the final size of the nanoparticles, but in that case, very different coercivities would be observed. An assembly of noninteracting and identical nanoparticles with volume V and magnetic anisotropy K would have zero coercivity above the blocking temperature T_B ($T_{B(A)} = 121$ K, $T_{B(B)} > 300$ K). In contrast, in the samples, the spread in K and V leads to a range of T_B and the existence of a finite coercivity at 300 K. Thus, apart from or along with the fact that different sizes of the nanoparticles formed inside the capsules, we should take into account the oxidation at their surface (the Ni^0/Ni^{2+} ratio in the nanoparticle composition, as already mentioned) and the distance in between (which defines the strength of interparticle interactions).

The magnetic interactions can be rather strong between the bare nanoparticles formed, as this mechanism of formation lacks of any type of molecules at their surface. This situation favors dipole–dipole interactions owing to the proximity of adjacent particles, and exchange interactions across grain boundaries can also be established, altering the anisotropy energy barrier E_B and causing a shift in the blocking temperature of the ZFC curve towards higher temperatures. Additionally, there is also a tendency toward increased broadening of the peak.[38] The presence of strong magnetic interactions in both samples is indeed inferred from the ZFC–FC curves because the temperature at which irreversibility between them takes place at high temperature ($T_{irr} > 200$ K in sample A and $T_{irr} > 300$ K in sample B). This T_{irr} is quite close to T_B, despite the fact of the very broad peak (generally associated to nanoparticles polydispersity) shown in the ZFC curve. Furthermore, in both cases, the FC curve reaches a plateau as decreasing temperature. As both samples are composed of small primary nanocrystals, they retain the superparamagnetic behavior at room temperature (almost no coercivity), but in view of the magnetic interactions established they show much higher saturation magnetization than individual nanodots[39] and a higher T_B.

In summary, we have reported the effective preparation of highly active nanoreactors based on the encapsulation of Pt_d nanoparticles inside hollow porous silica capsules. Especially relevant is the fact that the catalytic activity of these Pt_d nanoparticles is preserved after the encapsulation process. Furthermore, these nanoreactors are not just useful for the performance of chemical reactions in organic solvents by means of the easy functionalization of silica and its later dispersion in these solvents, but also for the fabrication of confined materials. Thus, making use of the catalytic activity of the Pt_d nanoparticles, different metals can be reduced inside the capsules, which may provide different synthetic advantages, such as the formation of new catalysts inside the nanoreactor that would otherwise be difficult and/or the addition of extra functionalities. As a proof of concept, Ni nanoparticles were synthesized in the inner cavity of the system, leading to the formation of an interesting type of

composites with tunable magnetic properties. The interest of these Ni-based composites lies in both their capability to be manipulated through an external magnetic field and the excellent catalytic properties of this metal.[40–42]

Experimental Section

All chemicals were of analytical grade and used without further purification.

Polystyrene (PS) beads (600 nm, Microparticles GmbH, 0.018 standard deviation) were coated with four alternating polyelectrolyte monolayers by using the electrostatic self-assembly layer-by-layer method.[24] The PS nanoparticles were firstly grafted with polystyrene sulfonate (PSS), a negatively charged polyelectrolyte. Poly(allylamine hydrochloride) (PAH) as positively charged polyelectrolyte was then grafted onto the particles. This process was repeated in order to obtain PS grafted with four layers of polymers (PS/PSS/PAH/PSS/PAH). Four layers of polyelectrolytes were chosen instead of two to improve the homogeneity of the coating shell and generate the positive surface charge (zeta potential, $\xi = +40$ mV) necessary for the electrostatic adsorption of 20–30 nm dendritic Pt (Pt_d) nanoparticles ($\xi = -20$ mV).

The Pt_d nanoparticles to be deposited onto the PS surface were synthesized as described elsewhere.[26] Briefly, sodium borohydride (1.22 mL, 0.02 M) was added as a reducing agent to a solution of sodium citrate (1.25 mL, 0.1 M) and K_2PtCl_4 (1.25 mL, 0.1 M) in ultrapure water (21.5 mL) and the resulting solution stirred for 10 min. For Pt deposition on the PS surface, PS@PSS/PAH/PSS/PAH (5 mg mL^{-1}) was added to a solution of Pt seeds (25.2 mL, 4.96 mM), and 1 h later the solution was centrifuged (20 min, 5000 rpm) and redispersed in pure water (20 mL) resulting in the removal of non deposited and free Pt dendritic nanoparticles.

Silica coating to give PS@Pt_d@SiO_2 was carried out following the method described by Graf et al.[43] Briefly, of polyvinylpyrrolidone (PVP; 1.5 mL, 110 mg mL^{-1}; MW = 40000) was added to a PS@Pt dendritic suspension (5 mL, 1.25 mg PS mL^{-1}). Two hours later, the suspension was washed three times by centrifugation at 3000 rpm, the sediment resuspended in 10 mL of a solution of NH_4OH in ethanol 4.2% (v/v), and sonicated for 5 min. A solution of tetraethoxysilane (TEOS) in ethanol (43.5 μL, 10% v/v) was then added to the suspension, centrifuged three times, and washed with water.

Hollow capsules of Pt_d@SiO_2 were fabricated by dissolving PS cores, which was achieved by shaking the bead suspension in an 1:1 ethanol/chloroform mixture in an orbital shaker for three days. Hollow capsules were washed and centrifuged three times, the first two with ethanol and then with water.

To obtain magnetic hollow structures of Ni-Pt_d@SiO_2 by confined growth of metal NPs, the Pt_d@SiO_2 dispersion (0.5 mg capsules mL^{-1}) was added to an aqueous solution (10 mL) containing a quantitative amount of $NiCl_2$ and hydrazine. Thus, $NiCl_2$ (1.7×10^{-2} M) and hydrazine (0.35 M) was used for sample A, and $NiCl_2$ (2.1×10^{-2} M) and hydrazine (0.39 M) for sample B. The mixture was maintained at 40 °C for 2 h, then centrifuged (4000 rpm, 15 min) and washed with water and ethanol (twice with each solvent).

TEM images were obtained using a JEOL JEM 1010 transmission electron microscope operating at an acceleration voltage of 100 kV. HRTEM, STEM, and elemental mapping by XEDS analysis were carried out with a JEOL JEM 2010F transmission electron microscope operating at an acceleration voltage of 200 kV. A vibrating sample magnetometer (VSM) was employed for the magnetic characterization.

Received: July 27, 2011
Revised: November 2, 2011
Published online: February 3, 2012

Keywords: nanocapsules · nanoreactors · porous materials · silica

[1] K. Renggli, P. Baumann, K. Langwoska, O. Onaca, N. Bruns, W. Meier, *Adv. Funct. Mater.* **2011**, *21*, 1241.
[2] L. L. del Mercato, P. Rivera-Gil, A. Z. Abbasi, M. Ochs, C. Ganas, I. Zins, C. Sönnichsen, W. Parak, *Nanoscale* **2010**, *2*, 458.
[3] G. B. Sukhorukov, A. L. Rogach, B. Zebli, T. Liedl, A. G. Skirtach, K. Koehler, A. A. Antipov, N. Gaponik, A. S. Susha, M. Winterhalter, W. J. Parak, *Small* **2005**, *1*, 194.
[4] J. T. Russell, Y. Lin, A. Böker, L. Su, P. Carl, H. Zettl, J. He, K. Sill, R. Tangirala, T. Emrick, K. Littrell, P. Thiyagarajan, D. Cookson, A. Fery, Q. Wang, T. P. Russell, *Angew. Chem.* **2005**, *117*, 2472; *Angew. Chem. Int. Ed.* **2005**, *44*, 2420.
[5] G. Y. Chai, W. B. Krantz, *J. Membr. Sci.* **1994**, *93*, 175.
[6] R. Ameloot, F. Vermoortele, W. Vanhove, M. B. J. Roeffaers, B. F. Sels, D. E. De Vos, *Nat. Chem.* **2011**, *3*, 382.
[7] V. Salgueiriño-Maceira, M. A. Correa-Duarte, *Adv. Mater.* **2007**, *19*, 4131.
[8] P. Evelyne, M. Estibaliz, D. Urbano, B. Daniel, C. Avelino, *J. Phys. Chem. C* **2011**, *115*, 7573.
[9] G. Fei, P. Botella, A. Corma, J. Blesa, L. Dong, *J. Phys. Chem. B* **2009**, *113*, 1796.
[10] J. Shin, R. M. Anisur, M. K. Ko, G. H. In, J. H. Lee, I. S. Lee, *Angew. Chem.* **2009**, *121*, 327; *Angew. Chem. Int. Ed.* **2009**, *48*, 321.
[11] J. Kim, J. E. Lee, J. Lee, J. H. Yu, B. C. Kim, K. An, Y. Hwang, C.-H. Shin, J.-G. Park, J. Kim, T. Hyeon, *J. Am. Chem. Soc.* **2006**, *128*, 688.
[12] Y. F. Zhu, J. L. Shi, W. H. Shen, X. P. Dong, J. W. Feng, M. L. Ruan, Y. S. Li, *Angew. Chem.* **2005**, *117*, 5213; *Angew. Chem. Int. Ed.* **2005**, *44*, 5083.
[13] L. J. Murray, M. Dinca, J. R. Long, *Chem. Soc. Rev.* **2009**, *38*, 1294.
[14] A. Corma, H. Garcia, F. X. L. Xamena, *Chem. Rev.* **2010**, *110*, 4606.
[15] O. P. Tiourina, A. A. Antipov, G. B. Sukhorukov, N. I. Larionova, Y. Lvov, H. Mohwald, *Macromol. Biosci.* **2001**, *1*, 209.
[16] E. W. Stein, D. V. Volodkin, M. J. McShane, G. B. Sukhorukov, *Biomacromolecules* **2006**, *7*, 710–719.
[17] S. Shimomura, M. Higuchi, R. Matsuda, K. Yoneda, Y. Hijikata, Y. Kubota, Y. Mita, J. Kim, M. Takata, S. Kitagawa, *Nat. Chem.* **2010**, *2*, 633.
[18] J. B. Fei, Y. Cui, X. H. Yan, W. Qi, Y. Yang, K. W. Wang, Q. He, J. B. Li, *Adv. Mater.* **2008**, *20*, 452.
[19] J. Liu, F. Liu, K. Gao, J. S. Wu, D. F. Xue, *J. Mater. Chem.* **2009**, *19*, 6073.
[20] M. Sanles-Sobrido, W. Exner, L. Rodríguez-Lorenzo, B. Rodríguez-González, M. A. Correa-Duarte, R. Álvarez-Puebla, L. M. Liz-Marzan, *J. Am. Chem. Soc.* **2009**, *131*, 2699.
[21] S. Mandal, M. Sathish, G. Saravanan, K. K. R. Datta, Q. Ji, J. P. Hill, H. Abe, I. Honma, K. Ariga, *J. Am. Chem. Soc.* **2010**, *132*, 14415.
[22] A. Shukla, P. Degen, H. Rehage, *J. Am. Chem. Soc.* **2007**, *129*, 8056.
[23] Y. Deng, Y. Cai, Z. Sun, J. Liu, C. Liu, J. Wei, W. Li, C. Liu, Y. Wang, D. Zhao, *J. Am. Chem. Soc.* **2010**, *132*, 8466.
[24] D. G. Shchukin, I. L. Radtchenko, G. B. Sukhorukov, *Mater. Lett.* **2003**, *57*, 1743.
[25] E. Donath, G. B. Sukhorukov, F. Caruso, S. A. Davis, H. Mohwald, *Angew. Chem.* **1998**, *110*, 2323; *Angew. Chem. Int. Ed.* **1998**, *37*, 2201.
[26] F. Caruso, R. A. Caruso, H. Mohwald, *Science* **1998**, *282*, 1111.
[27] A. L. Rogach, N. Gaponik, J. M. Lupton, C. Bertoni, D. E. Gallardo, S. Dunn, N. L. Pira, M. Paderi, P. Repetto, S. G.

Romanov, C. O. Dwyer, C. M. S. Torres, A. Eychmuller, *Angew. Chem.* **2008**, *120*, 6638; *Angew. Chem. Int. Ed.* **2008**, *47*, 6538.
[28] M. Sanles-Sobrido, V. Salgueiriño-Maceira, M. A. Correa-Duarte, L. M. Liz-Marzan, *Small* **2008**, *4*, 583.
[29] Z. W. Shan, G. Adesso, A. Cabot, M. P. Sherburne, S. A. S. Asif, O. L. Warren, D. C. Cherzan, A. M. Minor, A. P. Alivisatos, *Nat. Mater.* **2008**, *7*, 947.
[30] M. Sanles-Sobrido, M. A. Correa-Duarte, S. Carregal-Romero, B. Rodríguez-González, R. A. Álvarez-Puebla, P. Hervés, L. M. Liz-Marzán, *Chem. Mater.* **2009**, *21*, 1531.
[31] T. S. Ahmadi, Z. L. Wang, T. C. Green, A. Henglein, M. A. El-Sayed, *Science* **1996**, *272*, 1924.
[32] J. Chen, T. Herricks, Y. Xia, *Angew. Chem.* **2005**, *117*, 2645; *Angew. Chem. Int. Ed.* **2005**, *44*, 2589.
[33] M. A. Mahmoud, C. E. Tabor, M. A. El-Sayed, Y. Ding, Z. L. Wang, *J. Am. Chem. Soc.* **2008**, *130*, 4590.
[34] T. J. Freund, *Inorg. Nucl. Chem.* **1959**, *9*, 246.
[35] R. Narayanan, M. A. El-Sayed, *Nano Lett.* **2004**, *4*, 1343.
[36] M. Grzelczak, M. A. Correa-Duarte, V. Salgueiriño-Maceira, B. Rodríguez-González, J. Rivas, L. M. Liz-Marzán, *Angew. Chem.* **2007**, *119*, 7156; *Angew. Chem. Int. Ed.* **2007**, *46*, 7026.
[37] M. Sanles-Sobrido, M. Bañobre-López, M. A. Correa-Duarte, V. Salgueirino, B. Rodríguez-González, J. Rivas, L. M. Liz-Marzan, *J. Mater. Chem.* **2010**, *20*, 7360.
[38] S. Morup, F. Bodker, P. V. Hendriksen, S. Linderoth, *Phys. Rev. B* **1995**, *52*, 287.
[39] J. Ge, Y. Hu, Y. Yin, *Angew. Chem.* **2007**, *119*, 7572; *Angew. Chem. Int. Ed.* **2007**, *46*, 7428.
[40] I. S. Lee, N. Lee, J. N. Park, B. H. Kim, Y. W. Yi, T. Kim, P. K. Kim, I. H. Lee, S. R. Paik, T. Hydeon, *J. Am. Chem. Soc.* **2006**, *128*, 10658.
[41] N. Cordente, M. Respaud, F. Senocq, M. J. Casanove, C. Amiens, B. Chaudret, *Nano Lett.* **2001**, *1*, 565.
[42] J. Park, E. Kang, S. U. Son, H. M. Park, M. K. Lee, J. Kim, K. W. Kim, H. J. Hoh, J. H. Park, C. J. Bae, J.-G. Park, T. Hydeon, *Adv. Mater.* **2005**, *17*, 429.
[43] C. Graf, D. L. J. Vossen, A. Imhof, A. van Blaaderen, *Langmuir* **2003**, *19*, 6693.

